Pulsed Laser Deposition of Doped Lanthanum Gallate and In Situ Analysis by Mass Spectrometry of the Laser Ablation Plume

Tom Mathews, J. R. Sellar, and B. C. Muddle

Department of Materials Engineering, Monash University, Clayton 3168, Victoria, Australia

P. Manoravi*

Physikalisch-Chemisches Institut, University of Zürich, Irchel, Winterthurerstrasse 190, CH-8057, Zurich, Switzerland

Received June 1, 1999. Revised Manuscript Received October 14, 1999

Sr- and Mg-doped $LaGaO_3$ powders with various dopant concentrations ($La_{1-x}Sr_xGa_{1-y}Mg_yO_{3-(x+y)/2}$ where $0.02 \le x \le 0.2$ and $0.02 \le y \le 0.2$) were synthesized through a novel solution combustion route. X-ray diffraction patterns indicate orthorhombic structure for compositions $0 \le x \le 0.075$ and $0 \le y \le 0.075$ and primitive − cubic for $0.1 \le x \le 0.2$ and $0.1 \le y \le 0.2$. Thin films of $La_{1-x}Sr_xGa_{1-y}Mg_yO_{3-(x+y)/2}$ ($0.1 \le x \le 0.2$ and $0.1 \le y \le 0.2$) were deposited using both Nd:YAG (532 nm) and excimer (248 nm) lasers. The as-deposited films at room temperature were amorphous, which on annealing at 973 K exhibited single-phase cubic structure. Films deposited with excimer laser were smooth and particulate free compared to Nd:YAG laser deposition. The LSGM films on Si[111] and sapphire[0001] substrates showed good surface morphology compared to films on MgO[001] and amorphous quartz. Films were found to be slightly rich in Sr/La ratio compared to target composition. O^+, O, Ga^+, Ga, and La^+ were the major species in the laser ablation plume with ion and neutral velocities of 3×10^5 and 3×10^4 cm/s, respectively.

1. Introduction

Doped lanthanum gallate, $La_{1-x}Sr_xGa_{1-y}Mg_yO_{3-(x+y)/2}$ (LSGM), has been described as a superior oxide ion conductor with its ionic conductivity as high as about 0.1 S/cm at 1073 K[1−5] (comparable to that of yittria-stabilized zirconia, YSZ, at 1273 K) and is being envisaged for applications in reduced temperature solid oxide fuel cells operating at or below 1073 K.[1,5] However, the low mechanical strength of LSGM, especially at the fuel cell operating temperatures,[6] warrants the use of LSGM as thin film coatings on an electrode substrate. Conventionally, thin films are deposited using a vapor deposition technique. LSGM evaporates incongruently, and its constituents have very different vapor pressures, making it difficult to use the conventional physical vapor deposition techniques to produce thin films of desired stoichiometry. The metal−organic chemical vapor deposition process requires expensive organometallic compounds and knowledge of vapor pressures and other physicochemical properties to optimize the process parameters. Other techniques such as electrochemical vapor deposition and molecular beam epitaxy are likely to be cumbersome in the light of the material complexity.

Recently, pulsed laser deposition (PLD) has been successfully used to prepare thin films of oxides and nitrides of elements, stoichiometric and nonstoichiometric multicomponent oxides of complex structures such as the oxide superconductors, and several other electronic materials.[7] It is widely recognized as a powerful tool for depositing thin films of multicomponent systems. Besides, since the nanosecond laser pulses impinges the target surface and vaporize the material at the laser focused spot in a forced congruent manner, one would expect a stoichiometric deposition of thin films. In light of these advantages, in this paper, we describe our studies on the deposition of thin films of LSGM of various compositions using PLD technique along with their structural, morphological, and compositional characterization. Since the quality of the thin film obtained using PLD technique depends on the dynamics of the laser-induced plasma[8] (often called as laser plume), we also present the time-resolved mass spectroscopy analysis of the laser plume and the relative abundance of different neutral and charged species.

(1) Ishihara, T,; Matsuda, H.; Takita, Y. *J. Am. Chem. Soc.* **1994**, *116*, 3801.
(2) Feng, M.; Goodenough, J. B. Eur. *J. Solid State Inorg. Chem.* **1994**, *31*, 663.
(3) Huang, K.; Feng, M.; Goodenough, J. B.; Schmerling, M. *J. Electrochem. Soc.* **1996**, *144*, 3630.
(4) Huang, P.; Petric, A. *J. Electrochem. Soc.* **1996**, *143*, 1644.
(5) Huang, K.; Tichy, R. S.; Goodenough, J. B. *J. Am. Ceram. Soc.* **1998**, *81*, 2565.
(6) Drennan, J.; Zelizko, V.; Hay, D.; Ciacchi, F. T.; Rajendran, S.; Badwal, S. P. S. *J. Mater. Chem.* **1997**, *7*, 79.
(7) Chrisey, D. B.; Hubler, G. K. *Pulsed Laser Deposition of Thin Films*; Wiley: New York, 1994.
(8) Hastie, J. W.; Paul, A. J.; Bonnell, D. W.; Schenck, P. K. In Situ Monitoring by Mass Spectrometry of Laser Ablation Plumes Used in Thin Film Deposition. In *Synthesis and Characterization of Advanced Materials*; Serio, M. A., Gruen, M. D., Malhotra, R., Eds.; ACS Symp. Series, 681; American Chemical Society: Washington, DC, 1998; p 39.

10.1021/cm990341f CCC: $19.00
Published on Web 03/10/2000

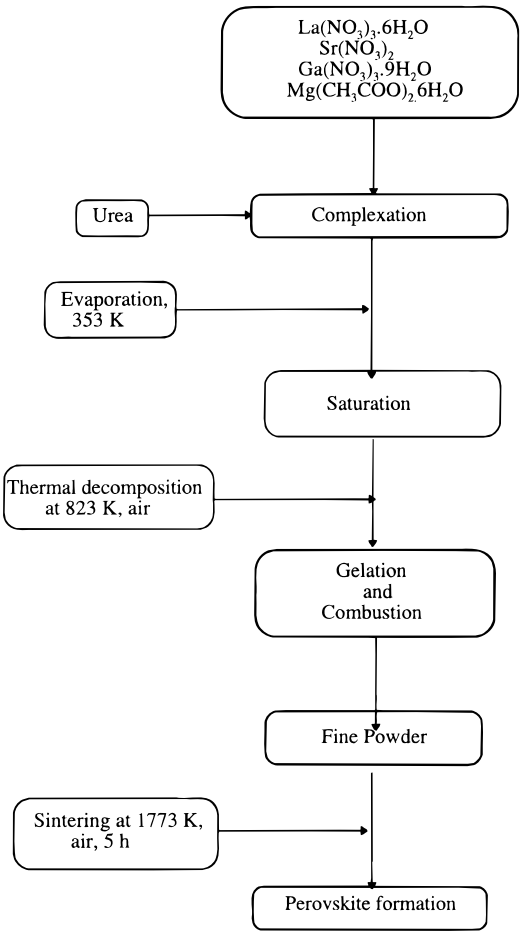

Figure 1. Flowchart of the solution combustion synthesis of LSGM.

2. Experimental Section

2.1. Bulk Material Preparation. Single-phase LSGM samples of various compositions were prepared, through a novel solution combustion synthesis technique, as shown in the flowchart of Figure 1. Appropriate amounts of lanthanum nitrate (99.9%), strontium nitrate (99.99%), gallium nitrate (99.9%), and magnesium acetate were dissolved in distilled water. The solution was saturated at 353 K followed by addition of urea as fuel and complexant. The amount of urea added was that required to consume completely the excess oxygen in the nitrate mixture and is called stoichiometric amount.[9,10] The solution was then refluxed for 10 min and introduced into an open muffle furnace maintained at 823 K. At this temperature excess water is removed from the solution resulting in the formation of a gel and its simultaneous combustion. The resulting fine powder was then pelletized by cold pressing and sintered at 1773 K for 5 h. The single-phase character of the final product was then confirmed by X-ray diffraction (XRD). The pellet density after sintering as measured by a pycnometer was 96% of the theoretical density.

2.2. Thin-Film Fabrication. High-density LSGM pellets prepared as above (20 mm diameter and 4 mm thickness) were used as targets for laser ablation. Thin film deposition was carried out using the laser-induced vaporization facility shown schematically in Figure 2. A Q switched Nd:YAG laser operating at 532 nm, having a pulse width of 8 ns (fwhm) with 80 mJ pulse energy was used for ablation. The details of the facility are given elsewhere.[11] Laser beam was focused on to the target at 45° normal to the target surface and the target was scanned in $x-y$ direction at a speed of 2 mm per minute in order to minimize the crater effects due to continuous irradiation of laser pulses. Films were deposited on quartz, Si[111], sapphire[0001], and MgO[001] substrates at room temperature with a target to substrate distance of 40 mm on-axis to the plume. A base pressure of 10^{-9} atm was maintained throughout the experiment. Depositions were carried out at different laser power densities in the range 10^7 to 10^9 W/cm^2 (fluence 0.1−10 J/cm^2) and good films were obtained for the power density 1.6×10^8 W/cm^2 (fluence 1.3 J/cm^2). Film depositions were also carried out under different oxygen background pressures. Since the ablation mechanism influences the morphology and structure of the resulting film,[12] and particulate-free films were not obtained using Nd:YAG laser, another set of ablation studies was carried out using a KrF excimer laser (248 nm). The excimer laser power density was optimized to 1.8×10^8 W/cm^2 (fluence 3 J/cm^2). Experimental conditions such as pulse repetition rate and target-to-substrate distance were maintained similar to that of Nd:YAG laser ablation.

2.3. Plume Analysis. The plume of Nd:YAG laser ablation at the laser fluence used for film deposition was subjected to mass analysis. The substrate holder shown in Figure 2 was removed from the ablation chamber to facilitate sampling of the molecular beam. The ablation chamber and the mass spectrometer chamber were differentially pumped to 10^{-9} and 10^{-11} atm, respectively. The time of arrival (TOA) signal of the ablation species, selected by a molecular beam skimmer, was fed to a Digital storage oscilloscope (DSO) and were averaged over 1000 laser shots to get better signal-to-noise ratio. The TOA profile of the ions was collected by turning off the ionizer of the QMS to avoid contribution from neutrals. Whereas, the signal for the neutrals was collected after deflecting away the ions by employing a pair of parallel deflecting plates with suitable electrical biasing in the "flight" path of the species. The TOA profile recorded in DSO was deconvoluted from the detector time response[13] for further analysis. For ion species the velocity obtained was of the order of 3×10^5 cm/s, whereas for the neutral species it varied from 2.5×10^4 to 5×10^4 cm/s. The large velocity for the ions are understandable in view of the high kinetic energy acquired by the ions because of the space-charge field near the target surface and the inverse Bremsstrahlung type of absorption of the trailing part of the laser pulse by the ions. The velocities of the neutral species were mass dependent. It has been shown that[13,14,15] during laser ablation under thermal regime the neutral species are evaporated by the surface temperature rise due to the laser pulse heating. The evaporated species undergo a local thermal equilibrium[13,15] with the surface temperature and hence acquire kinetic energy accordingly.

The major species present in the plume are O^+, Ga^+, La^+, O, and Ga. Other species observed are Mg^+, Mg, MgO^+, MgO, Mg_2O, Sr^+, Sr, SrO^+, SrO, La, LaO^+, LaO, Ga_2O^+, and Ga_2O. The species distribution present in the plume is shown in Figure 3. The intensity of each species in Figure 3 is corrected for its isotopic abundance,[14] ionization cross section,[16] and ion transmission coefficient.[17] Since the ablation at high laser fluences produced severe particulate deposition in thin films, high fluence plumes were not characterized by mass spectrometry.

(9) Muthuram, M.; Arul Dhas, N.; Patil, K. C. *Bull. Mater. Sci.* **1994**, *17*, 977.
(10) Ekambaram, S.; Patil, K. C. *J. Mater. Chem.* **1995**, *5*, 905.
(11) Joseph, M.; Sivakumar, N.; Darwin Albert Raj, D.; Mathews, C. K. *Rapid Commun. Mass. Spectrosc.* **1996**, *10*, 5.
(12) Kautek, W.; Roas, B.; Schultz, L. *Thin Solid Films* **1990**, *191*, 191.
(13) Joseph, M.; Sivakumar, N.; Darwin Albert raj, D.; Mathews, C. K. *J. Nucl. Mater.* **1997**, *247*, 21.
(14) Joseph, M.; Sivakumar, N.; Manoravi, P. *Int. J. Mass Spectrom. Ion Processes* **1998**, *176*, 237.
(15) Hastie, J. W.; Bonnell, D. W.; Schenk, P. K. *High Temp.-High Press.* **1998**, *20*, 73.
(16) Bonnell, D. W. Software "SIGMA", version 1.1; NIST: Gaithersburg, MD, 1990.
(17) Bonnel, D. W.; Hastie, J. W. *Characterization of High-Temperature Vapours and Gases*, Hastie, J. W., Ed.; Proc. 10th Mater. Res. Symp; NBS sp-561/1; US Gov. Printing Office: Washington, DC, 1979; p 537.

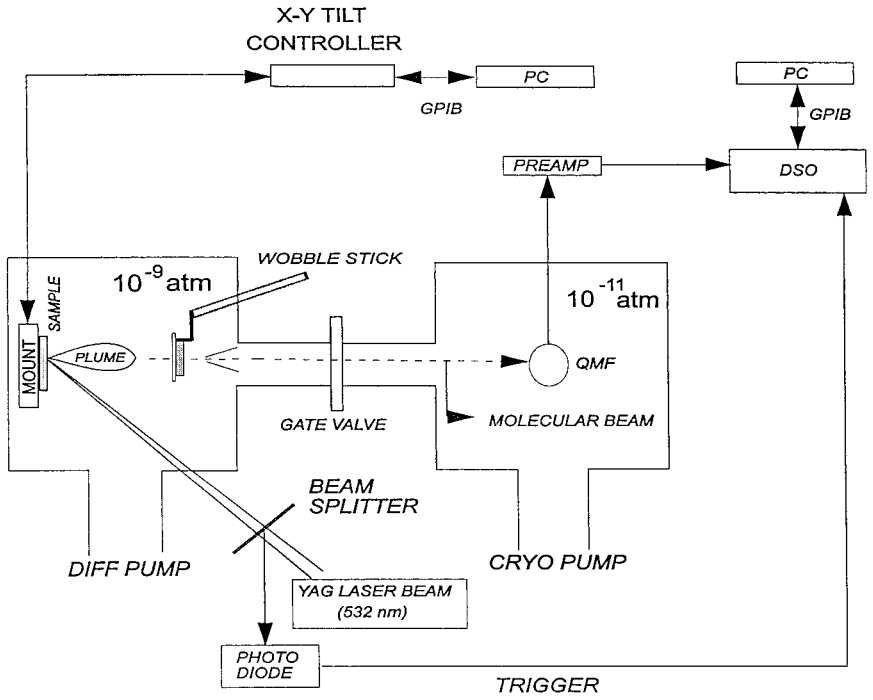

Figure 2. Schematic representation of the thin-film deposition and laser plume analysis by quadrupole mass spectrometry.

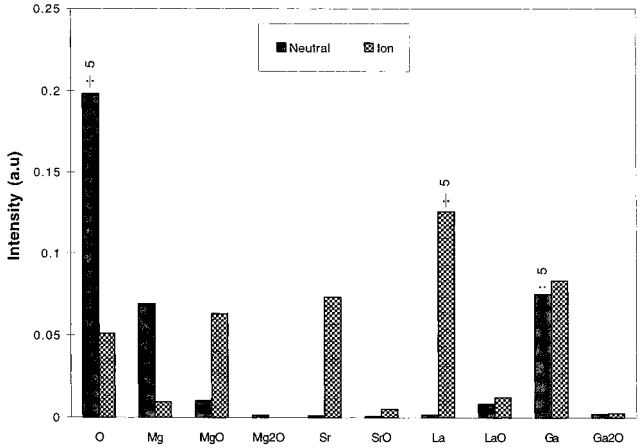

Figure 3. Intensity of different species in the Nd:YAG laser plume from $La_{0.8}Sr_{0.2}Ga_{0.85}Mg_{0.15}O_{2.825}$ target detected in QMS. The intensities are corrected for the isotopic abundance, ionization cross section for the neutrals, and mass transmission coefficients.

3. Results and Discussion

The parent compound $LaGaO_3$ shows a high degree of tolerance for defects in the oxygen sublattice and has an orthorhombic structure. With the substitution of La^{3+} with Sr^{2+} and Ga^{3+} with Mg^{2+} the lattice parameters systematically change until eventually the cubic structure results. Table 1 shows the compositions studied and the corresponding structures observed. Single-phase perovskite structure was obtained for all compositions studied. The XRD pattern obtained for each composition in the range $0.1 \leq x \leq 0.2$ and $0.1 \leq y \leq 0.2$ were identical and akin to that reported for the composition $La_{0.9}Sr_{0.1}Ga_{0.8}Mg_{0.2}O_{2.85}$ by various groups.[1,2,4,6] The powder XRD pattern of $La_{0.9}Sr_{0.1}Ga_{0.85}Mg_{0.15}O_{2.825}$, the composition corresponding to the highest oxide ion conductivity[4] is shown in Figure 4. The indexed XRD data for $La_{0.9}Sr_{0.1}Ga_{0.85}Mg_{0.15}O_{2.825}$ is shown in Table 2.

Table 1. Crystal Structures of Some Sr- and Mg-Doped $LaGaO_3$ Compositions

composition	crystal structure
$LaGaO_3$	orthorhombic
$La_{0.98}Sr_{0.02}Ga_{0.98}Mg_{0.02}O_{2.98}$	orthorhombic
$La_{0.95}Sr_{0.05}Ga_{0.95}Mg_{0.05}O_{2.95}$	orthorhombic
$La_{0.925}Sr_{0.075}Ga_{0.925}Mg_{0.075}O_{2.925}$	orthorhombic
$La_{0.9}Sr_{0.1}Ga_{0.9}Mg_{0.1}O_{2.9}$	cubic
$La_{0.9}Sr_{0.1}Ga_{0.85}Mg_{0.15}O_{2.875}$	cubic
$La_{0.9}Sr_{0.1}Ga_{0.8}Mg_{0.2}O_{2.85}$	cubic
$La_{0.9}Sr_{0.1}Ga_{0.75}Mg_{0.25}O_{2.825}$	cubic
$La_{0.85}Sr_{0.15}Ga_{0.9}Mg_{0.1}O_{2.875}$	cubic
$La_{0.85}Sr_{0.15}Ga_{0.85}Mg_{0.15}O_{2.85}$	cubic
$La_{0.85}Sr_{0.15}Ga_{0.8}Mg_{0.2}O_{2.825}$	cubic
$La_{0.8}Sr_{0.2}Ga_{0.9}Mg_{0.1}O_{2.85}$	cubic
$La_{0.8}Sr_{0.2}Ga_{0.85}Mg_{0.15}O_{2.825}$	cubic
$La_{0.8}Sr_{0.2}Ga_{0.8}Mg_{0.2}O_{2.8}$	cubic

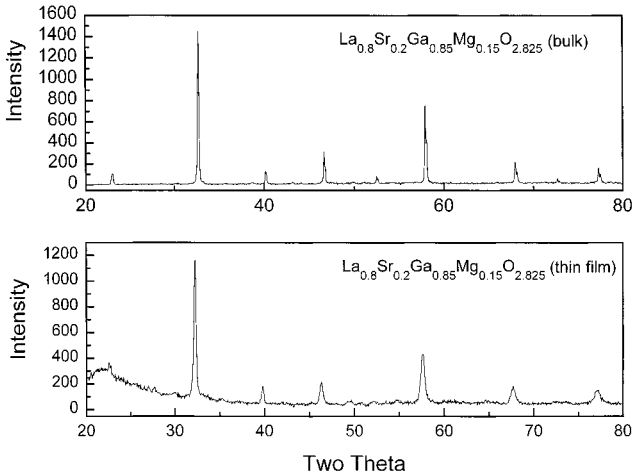

Figure 4. XRD pattern of bulk and thin film of $La_{0.8}Sr_{0.2}Ga_{0.85}Mg_{0.15}O_{2.825}$.

The XRD pattern of the vacuum-deposited, annealed film corresponding to the target composition $La_{0.9}Sr_{0.1}Ga_{0.85}Mg_{0.15}O_{2.825}$ is compared with that of the bulk in

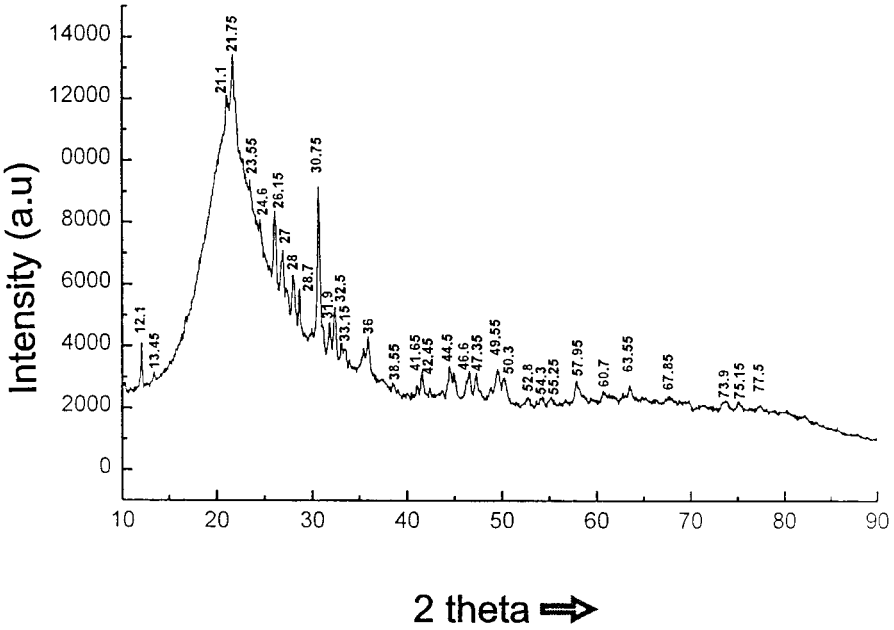

Figure 5. XRD pattern of the thin film deposited under 2.6×10^{-4} atm of oxygen. Some peaks in this pattern could not be indexed.

Table 2. Powder Diffraction Data for $La_{0.8}Sr_{0.2}Ga_{0.85}Mg_{0.15}O_{2.825}$

2θ, deg	d, Å (obsd)	I/I_o	hkl
22.74	3.917	8	100
32.35	2.767	100	110
39.9	2.259	10	111
46.4	1.957	20	200
52.25	1.7508	04	210
57.7	1.5977	50	211
67.7	1.3840	15	220
72.45	1.3045	3	300
77.05	1.2377	12	310
81.55	1.1804	6	311
86.05	1.1304	10	222

Figure 4. Similar patterns were obtained for all the films corresponding to the 10 compositions studied. The hump seen in the XRD pattern of the thin film in the 2θ range 20−30° is that of the quartz substrate, which has been verified by recording the XRD pattern of the substrate alone. Diffraction pattern for both bulk and thin films were similar except for the absence of two minor peaks at $2\theta = 52.35$ and 77.17° in the thin film. This is understandable in principle as the amount of materials in the thin films is much less and the peak intensity is a function of the quantity of the material exposed to X-ray radiation.

The X-ray studies showed that the as-deposited films were amorphous, suggesting that the kinetics of crystal growth on the substrate at room temperature during film deposition could be sluggish. The films deposited under high vacuum, corresponding to the 10 compositions ($0.1 \leq x \leq 0.2$; $0.1 \leq x \leq 0.2$) given in Table 1, upon annealing at 973 K for 3 h, gave single-phase perovskite LSGM. Whereas the films deposited under oxygen background upon annealing showed mixture of phases (Figure 5), some of the diffraction peaks of this mixed phase film could not be indexed. The ablation species are mostly rare earth atoms and ions having high kinetic energy in the range 5−7 eV. Under sufficient background oxygen pressure, these high-energy species collide with the oxygen molecules before reaching the substrate. These high-energy collisions may lead to the formation of oxide phases and their subsequent deposition on the substrate. This could be a possible explanation for the unindexed peaks in the XRD pattern of the films grown under background oxygen partial pressures.

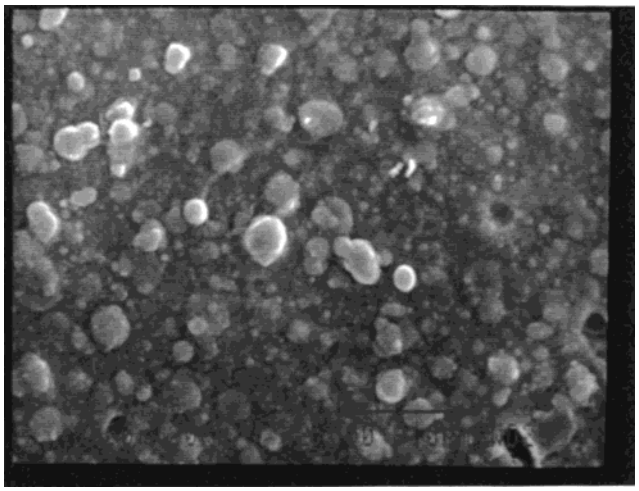

Figure 6. SEM picture of the annealed film deposited from $La_{0.8}Sr_{0.2}Ga_{0.85}Mg_{0.15}O_{2.825}$ target on amorphous quartz substrate. (Magnification: ×2000. Full scale length in x direction: 45 μm.)

Figure 6 displays the SEM picture of a typical annealed film grown on quartz substrate from $La_{0.9}Sr_{0.1}Ga_{0.85}Mg_{0.15}O_{2.825}$ target using Nd:YAG laser. Presence of particulates and microcracks are observed in certain areas. No microcracks were observed in the as-deposited films. The microcracks are believed to have developed during annealing due to thermal expansion coefficient (TEC) mismatch between quartz and LSGM. The average TEC of amorphous quartz[18] in the temperature

(18) Touloukian, Y. S.; Kirby, R. K.; Taylor, R. E.; Lee, T. Y. R *Thermophysical Properties of Matterials*; IFI/Plenum: New York, 1977; Vol. 13, p 358.

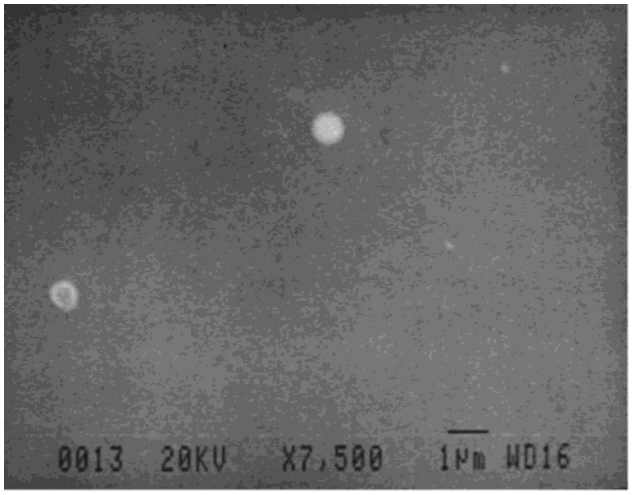

(a)

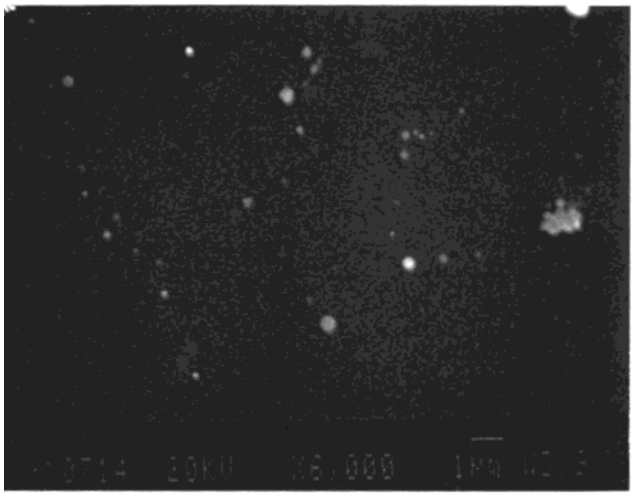

(b)

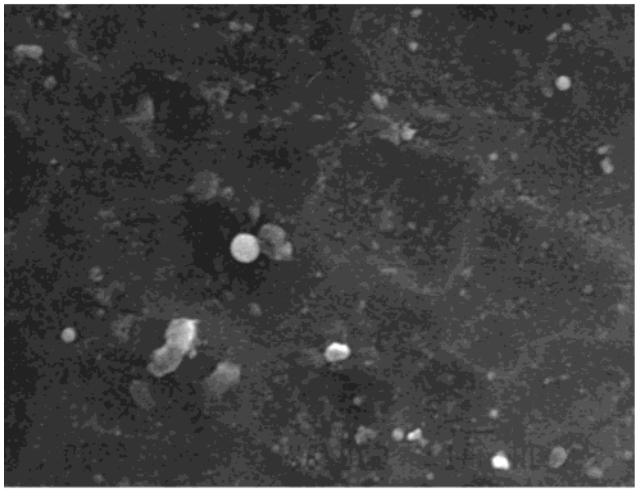

(c)

Figure 7. SEM pictures of annealed films deposited using KrF excimer laser on (a) Si[111] (magnification ×7500), (b) sapphire[0001] (magnification ×6000), and (c) MgO[001] (magnification ×6000) substrates. Full scale length in *x* direction: 20 μm.

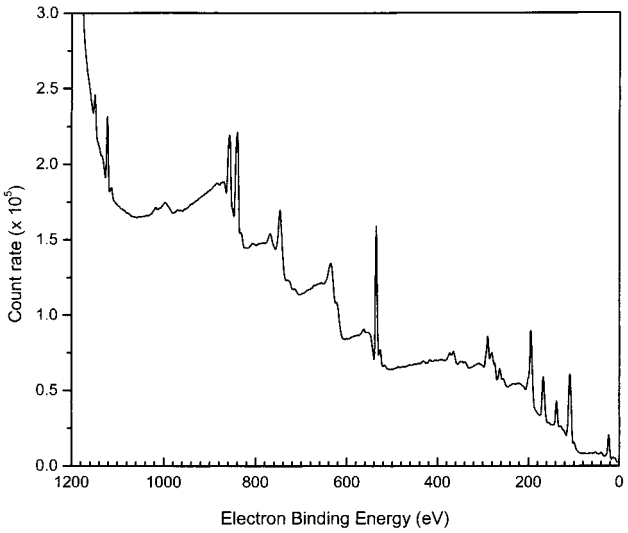

Figure 8. XPS spectrum of film deposited from $La_{0.8}Sr_{0.2}Ga_{0.85}Mg_{0.15}O_{2.825}$ target using Mg Kα as X-ray source. The various peaks are indexed in Table 3. The peaks at 746 and 766 are the Auger lines of oxygen and the peak at 635 is the Auger line of La due to Mg Kα source.

range 773−1273 K is ∼0.42 × 10^{-6} K^{-1}. The TEC of bulk $La_{0.9}Sr_{0.1}Ga_{0.85}Mg_{0.15}O_{2.825}$ was determined from the lattice parameter values using high-temperature powder XRD in the temperature range 298−1273 K at the interval of 100 K. Al_2O_3 obtained from National Institute of Standards and Technology, Gaithersburg, MD was used as the internal standard. The result obtained for the above composition is 11.6 × 10^{-6} K^{-1}. This value is close to that obtained by Stevenson et al.[19] (11.5 × 10^{-6} K^{-1}) and is slightly higher than that of YSZ (10.3 × 10^{-6} K^{-1}). Feng and Goodenough[2] reported an average value of 10 × 10^{-6} K^{-1} for the same compound. The average TEC of LSGM is ∼28 times that of quartz. Since the TEC of Si and sapphire are relatively close to that of LSGM compared to quartz, LSGM film deposition is preferred on these substrates.

Figure 7a−c compare the SEM pictures of films from $La_{0.8}Sr_{0.2}Ga_{0.85}Mg_{0.15}O_{2.825}$ target deposited on Si [111], sapphire [0001], and MgO [001] substrates using an excimer laser. A smaller number of particulates were observed in films deposited using the excimer laser compared to Nd:YAG laser. This could be due to the shorter wavelength of the excimer laser. Under similar conditions, we obtained smooth films on Si [111] and sapphire [0001] substrates as compared to those grown on MgO [001] and quartz substrates. While the Nd:YAG laser deposition over 12 000 laser shots produced a film thickness of 800 nm, the same thickness was obtained in 3600 excimer laser shots with similar power density. Hence, apart from minimal particulate deposition, excimer laser renders 3.3 times higher deposition rate than Nd:YAG laser.

The composition of the thin film obtained from the laser ablation of $La_{0.8}Sr_{0.2}Ga_{0.85}Mg_{0.15}O_{2.825}$ bulk sample was measured using X-ray photoelectron spectroscopy (XPS) with Mg Kα as X-ray source. The XPS spectrum is shown in Figure 8. The various peaks observed and the respective assignments are listed in Table 3. The

(19) Stevenson, J. W.; Armstrong, T. R.; McCready, D. E.; Pederson, L. R.; Weber, W. J. *J. Electrochem. Soc.* **1997**, *144*, 3613.

Table 3. Various Peaks Observed in the XPS Analysis (Figure 7) of Thin Film Deposited from the Target $La_{0.8}Sr_{0.2}Ga_{0.85}Mg_{0.15}O_{2.85}$ and Their Assignments

S no.	peak position (eV)	assignment
1	23.3	Ga (3d), Sr (4p)
2	39.4	Sr (4s)
3	52.8	Mg (2p)
4	105.6	La ($4d\ ^{5}/_{2}$, $4d\ ^{3}/_{2}$)
5	108.9	Ga ($3p\ ^{3}/_{2}$, $3p\ ^{1}/_{2}$)
6	138	Sr ($3d\ ^{5}/_{2}$, $3d\ ^{3}/_{2}$)
7	167.6	Ga (3s)
8	195.1	La ($4p\ ^{3}/_{2}$)
9	272.8	Sr ($3p\ ^{3}/_{2}$)
10	279.4	Sr ($3p\ ^{1}/_{2}$), La (4s)
11	289	C (1s)
12	364.8	Sr (3s)
13	532.8	O (1s)
14	838	La ($3d\ ^{5}/_{2}$)
15	855	La (3d 3/2)
16	1122.3	Ga (2p 3/2)
17	1147.9	Ga (2p 1/2)

carbon 1s peak observed at 289 eV in the binding energy scale is due to carbon contamination on the film surface. Since the XPS technique is very sensitive to the top layer such carbon impurity signal becomes unavoidable for samples exposed to the atmosphere for long time. For each element, nonoverlapping peaks were scanned individually in a high-resolution mode. The elemental compositions were then calculated from the area under the peaks, electron kinetic energy, and the subshell photoionization cross section corresponding to each peak using the quantization method described by Ratner and Castner.[20] The relative mole fraction of La and Sr (La/La + Sr and Sr/La + Sr) in the film is found to be 0.74 and 0.26, respectively, and that of Ga and Mg is 0.86 and 0.14, respectively. The atomic composition of La, Sr, Ga, Mg, and O is 13%, 4.7%, 18.7%, 3%, and 60.6%, respectively. These values correspond to the film composition $La_{0.74}Sr_{0.26}Ga_{0.86}Mg_{0.14}O_{3.03}$. The deposited film shows a higher O and Sr/La ratio compared to that of target ($La_{0.8}Sr_{0.2}Ga_{0.85}Mg_{0.15}O_{2.825}$). PLD process is well-known for its forced congruent evaporation and hence stoichiometric transfer of components from target to film[7] is expected. However, in the present material, the high laser power density to ensure forced congruent evaporation produced particulate deposition. At lower laser power density evaporation under thermal regime dominates in the plume and hence, apart from the sticking coefficient of different species, the film composition could also depend on the vaporization kinetics of the target material at the surface temperature due to laser heating. Sr has a higher vapor pressure compared to La and hence might lead to a Sr-rich film. The possibility of adsorbed oxygen on the film surface could be a reason for the higher oxygen fraction observed.

(20) Ratner, B.; Castner, D. Electron spectroscopy for chemical analysis. In *Surface Analysis − The principal technique*; Vickerman, J. C., Ed.; John Wiley and Sons: New York, 1997; p 43.

4. Summary

LSGM thin films were deposited by PLD technique using both Nd:YAG and KrF excimer lasers from high-density LSGM targets prepared by solution combustion synthesis. The laser plume contains constituent elements and oxides of ions and neutrals with velocities of 10^5 and 10^4 cm/s, respectively. Smoother films were obtained at a power density of 1.6×10^8 W/cm^2 (fluence 1.3 J/cm^2) for Nd:YAG and 1.8×10^8 W/cm^2 (fluence 3 J/cm^2) for excimer laser. Films deposited with excimer laser showed higher deposition rate and better quality in terms of particulate deposition compared to that of Nd:YAG laser. Even though epitaxial films are not required for the proposed application of LSGM films, the film surface morphology necessitates the use of appropriate substrates with matching thermal expansion coefficients. While XRD studies confirm the target phase formation in the film, XPS studies revealed that the films are slightly rich in Sr/La ratio.

CM990341F